HHS Public Access

Author manuscript

Neuropathol Appl Neurobiol. Author manuscript; available in PMC 2022 December 01.

Published in final edited form as:

Neuropathol Appl Neurobiol. 2021 December ; 47(7): 1033–1049. doi:10.1111/nan.12732.

Distinct brain-derived TDP-43 strains from FTLD-TDP subtypes induce diverse morphological TDP-43 aggregates and spreading patterns *in vitro* and *in vivo*

Sílvia Porta[1], **Yan Xu**[1], **Tagan Lehr**[1], **Bin Zhang**[1], **Emily Meymand**[1], **Modupe Olufemi**[1], **Anna Stieber**[1], **Edward B. Lee**[2], **John Q. Trojanowski**[1], **Virginia M.-Y. Lee**[1]

[1]Center for Neurodegenerative Disease Research (CNDR), Institute on Aging, Department of Pathology and Laboratory Medicine, University of Pennsylvania, Perelman School of Medicine, Philadelphia, PA, USA

[2]Translational Neuropathology Research Laboratory, Department of Pathology and Laboratory Medicine, Perelman School of Medicine, University of Pennsylvania, Philadelphia, PA, USA

Abstract

Aim: The heterogeneity in the distribution and morphological features of TAR DNA-binding protein-43 (TDP-43) pathology in the brains of frontotemporal lobar degeneration (FTLD-TDP) patients and their different clinical manifestations suggest that distinct pathological TDP-43 strains could play a role in this heterogeneity between different FTLD-TDP subtypes (A-E). Our aim was to evaluate the existence of distinct TDP-43 strains in the brains of different FTLD-TDP subtypes and characterise their specific seeding properties *in vitro* and *in vivo*.

Methods and Results: We used an inducible stable cell line expressing a mutant cytoplasmic TDP-43 (iGFP-NLSm) to evaluate the seeding properties of distinct pathological TDP-43 strains. Brain-derived TDP-43 protein extracts from FTLD-TDP types A ($n = 6$) and B ($n = 3$) cases induced the formation of round/spherical phosphorylated TDP-43 aggregates that morphologically differed from the linear and wavy wisps and bigger heterogeneous filamentous (skein-like) aggregates induced by type E ($n = 3$) cases. These morphological differences correlated with distinct biochemical banding patterns of sarkosyl-insoluble TDP-43 protein recovered from the transduced cells. Moreover, brain-derived TDP-43 extracts from type E cases showed higher

Correspondence Virginia M.-Y Lee and Sílvia Porta, Center for Neurodegenerative Disease Research (CNDR), Institute on Aging, Department of Pathology and Laboratory Medicine, Perelman School of Medicine, University of Pennsylvania, Philadelphia, PA 19104, USA. vmylee@upenn.edu; silviap@pennmedicine.upenn.edu.

AUTHORS CONTRIBUTIONS

S.P. designed, performed the experiments and analysed the data. Y.X., T.L. performed experiments and analysed the data; A.S. performed the EM studies. B.Z., E.M and M.O. performed stereotaxic injections; E.B.L. analysed the data and critically reviewed and edited the manuscript. J.Q.T. critically reviewed and edited the manuscript. S.P. and V.M.-Y. L wrote the manuscript.

CONFLICT OF INTEREST

The authors declare no competing interests.

ETHICAL APPROVAL

Informed consent was obtained from next of kin at the time of death.

PEER REVIEW

The peer review history for this article is available at https://publons.com/publon/10.1111/nan.12732.

SUPPORTING INFORMATION

Additional supporting information may be found online in the Supporting Information section.

susceptibility to PK digestion of full-length TDP-43 and the most abundant C-terminal fragments that characterise type E extracts.

Finally, we showed that intracerebral injections of different TDP-43 strains induced a distinctive morphological and subcellular distribution of TDP-43 pathology and different spreading patterns in the brains of CamKIIa-hTDP-43_{NLSm} Tg mice.

Conclusions: We show the existence of distinct TDP-43 strains in the brain of different FTLD-TDP subtypes with distinctive seeding and spreading properties in the brains of experimental animal models.

Keywords

frontotemporal lobar degeneration (FTLD); TDP-43; seeding; spreading; protein strains

INTRODUCTION

The intracellular mislocalisation and aggregation of phosphorylated TAR DNA-binding protein-43 (TDP-43) is the pathological hallmark of frontotemporal lobar degeneration with TDP-43 inclusions (FTLD-TDP) and nearly all the cases of amyotrophic lateral sclerosis (ALS).[1] The correlation between the neuropathological features of TDP-43 pathology, clinical symptoms and underlying genetics of FTLD-TDP has been extensively reported.[2–10] The distinctive distribution and morphology of TDP-43 pathology in cortical areas of FTLD-TDP cases defines five different subtypes (i.e. type A, B, C, D and E).[7,8,11] FTLD-TDP type A is characterised by abundant neuronal cytoplasmic inclusions (NCIs) and dystrophic neurites (DNs) in superficial cortical laminae. FTLD-TDP type A cases are associated with *Progranulin* (*GRN*) mutations and exhibit behavioural variant frontotemporal degeneration (bvFTD) or non-fluent/agrammatic PPA (naPPA). FTLD-TDP type B cases show compact NCIs with few DNs in both superficial and deep neocortical layers. This FTLD-TDP subtype is associated with *C9orf72* repeat expansion mutations (*C9+*) and bvFTD, including cases with motor-neuron disease (FTLD-MND). FTLD-TDP type C is characterised by long and thick DNs primarily in superficial cortical layers. Type C cases are typically sporadic and associated with bvFTD or semantic variant PPA (svPPA). FTLD-TDP type D exhibits lentiform neuronal intranuclear inclusions (NIIs) in superficial and deep cortical layers and few DNs. Type D cases are linked to *VCP* mutations and present with familial inclusion body myositis, Paget's disease of bone, FTD, and/or ALS (called multisystem proteinopathy).[3,9] Finally, FTLD-TDP type E exhibits granulofilamentous neuronal inclusions (GFNI's) and neuropil grains in superficial and deep neocortical layers, and abundant curvilinear oligodendroglial inclusions. This subtype has been seen in both sporadic and *C9+* cases and is clinically associated with bvFTD.[11]

The molecular mechanisms underlying such microregional and morphologic heterogeneity of TDP-43 pathology and their associated clinical manifestations remain unknown. This diversity in TDP-43 pathology suggests that distinct pathological TDP-43 protein conformations, also known as strains, could play a role in the clinical and pathological heterogeneity in FTLD-TDP. In this regard, strain-like properties of misfolded proteins have

been well described in other neurodegenerative diseases, including α-synucleinopthies,[12–14] Aβ amyloidosis,[15,16] tauopathies[17–19] and to some extent TDP-43 proteinopathies.[20–23]

The ability of pathological TDP-43 proteins obtained from post-mortem brain extracts to induce *de-novo* TDP-43 aggregates has been demonstrated *in vitro* and *in vivo*.[20,21,23–25] Cell-to-cell transmissibility of TDP-43 oligomers has been shown in cultured neurons, with retrograde transport from axonal terminals to the soma and anterograde transport from axonal terminals to interconnected cell populations.[21] Evidence that such cell-to-cell transmission can occur *in vivo* has been shown recently in experimental animal models.[20] Stereotaxic injections of human brain-derived TDP-43 extracts from FTLD-TDP cases into the brains of doxycycline (Dox)-regulatable transgenic (Tg) mice that express cytoplasmic human TDP-43 proteins[26–28] as well as in wild-type mice (WT), led to a time-dependent induction of TDP-43 aggregates in recipient mice.[20] Moreover, the propagation and spreading of TDP-43 pathology in a time-dependent manner was observed in the brains of CamKIIa-hTDP-43$_{NLSm}$ mice injected with human brain-derived pathological TDP-43 from the injection site to distal areas. The presence of TDP-43 pathology in interconnected brain regions supports the hypothesis of a transneuronal mechanism of spreading through the neuroanatomical connectome.

Here we show that pathological TDP-43 proteins or strains extracted from brains of different FTLD-TDP subtypes, when used as pathogenic seeds after introduction into a doxycycline-inducible cell line expressing GFP-tagged cytoplasmic TDP-43 protein (iGFP-NLSm),[20] differentially recruit TDP-43 into phosphorylated cytoplasmic aggregates with distinct morphological features. Moreover, we show that intracerebral injections of brain-derived TDP-43 strains into CamKIIa-hTDP-43$_{NLSm}$ Tg mice induce distinctive morphological, subcellular distributions and spreading patterns of TDP-43 pathology in the brain and suggest a novel mechanism of disease progression in FTLD-TDP.

MATERIALS AND METHODS

Autopsy cohort

Human post-mortem brains were obtained from the CNDR Brain Bank at the University of Pennsylvania.[29] All necessary informed consent forms were obtained from the patients or their next of kin at the time of death. Histopathologic subtyping of our FTLD-TDP cohort was conducted according to established guidelines.[7,8] Genetic testing for *GRN* mutations, *C9orf72* expansions and *TBK1* mutations was performed as previously described.[30–32] The genetic and demographic data of cases used in this study are summarised in Table S1.

Brain-derived TDP-43 protein extracts from FTLD-TDP cases

Brain-derived sarkosyl-insoluble TDP-43 proteins were obtained from human post-mortem brains by sequential extraction using buffers of increasing strength as described.[20] Briefly, grey matter from the frozen frontal cortex was extracted with 1% Triton X-100 high salt buffer (HS).[11,20] After myelin removal, the resulting pellet was treated with Benzonase and extracted with 2% sarkosyl-HS buffer. The pellet was washed and re-suspended with DPBS (Dulbecco's phosphate-buffered saline) by sonication using a hand-held probe (QSonica,

Newtown, CT). Finally, an additional spin at 5,000 x g for 5 min at 4°C was performed to remove large protein debris to obtain the final sarkosyl-insoluble fraction (sark-insoluble). Total protein concentration was measured by BCA assay (Thermo Scientific Inc., Rockford, IL), and TDP-43 protein concentration was determined using TDP-43 Enzyme-linked Immunosorbent Sandwich Assay (ELISA) (see supplementary Materials and Methods).

Maintenance of dox-inducible GFP-NLSm stable cell lines (iGFP-NLSm)

iGFP-NLSm stable cells (clone #6.B7) were maintained in Dulbecco's modified Eagle's medium (DMEM, Corning Cellgro, Manassas, VA) with 10% of tetracycline-screened FBS (Atlanta Biologicals, Flowery Branch, GA), 1% Penicillin-Streptomycin (Corning Cellgro, Manassas, VA) and L-glutamine (20 mM, Corning Cellgro, Manassas, VA) at 37°C in a humidified chamber containing 5% CO_2. Once a week, cells were maintained under selection conditions by adding G418 (400 μg/ml, Calbiochem, La Jolla, CA) and puromycin (2 μg/ml, MilliporeSigma, St Louis, MO).

In vitro TDP-43 seeding assay

Brain-derived sarkosyl-insoluble extracts were sonicated using a hand-held probe (3 × 10 pulses, intensity 2.5, QSonica, Newtown, CT) and equivalent amounts of insoluble TDP-43 protein i.e. 0.25–0.3 ng (24-MW plates), 1–1.2 ng (6-MW plates), according to ELISA (C89) measures (Table S2), were transduced into iGFP-NLSm cells using Bioporter® as a protein delivery reagent (BP509696, Genlantis, San Diego, CA) as previously described.[20] Protein-B ioporter® complexes were added to the cells and incubated for 4 h. Cells were placed back on fresh medium in the absence or presence of doxycycline (Dox, 1.0 μg/ml) and cultured for 1, 2 or 3 additional days depending on the experimental approach. Cell culture experiments were blinded with respect to the patient-derived brain extracts used for transduction and posterior analysis.

Sequential biochemical fractionation of cell extracts

iGFP-NLSm cells were plated in 6-MW plates (1.5×10^5 cells) and proteins were extracted 3 days post-transduction as described previously.[20] The final sarkosyl-insoluble pellet was resuspended in 50 μl of DPBS by sonication and saved as sark-insoluble fraction.

Mouse cohorts

Heterozygous and homozygous tetO-hTDP-43_{NLSm} mice were bred with CamKIIa-tTA mice to generate bigenic mice, as described previously.[26–28] Both male and female adult mice (3–5 months old) were used for this study. Mice were maintained with chow containing Dox (200 mg/kg, Dox Diet, S3888; Bio-Serv., Flemington, NJ). Transgene expression was induced by switching to standard chow lacking Dox (Rodent Diet 20 #5053, PicoLab, St. Louis, MO). All breeding, housing and procedures were performed following the NIH Guide for the Care and Use of Experimental Animals. Studies were approved by the Institutional Animal Care and Use Committee of the University of Pennsylvania (IACUC).

Stereotaxic surgery on mice

One week prior to stereotaxic surgery the CamKIIa-hTDP-43$_{NLSm}$ mice were switched to standard chow to induce transgene expression. Stereotaxic surgery was performed as described previously.[20,33] Sark-insoluble brain extracts were sonicated (6 × 10 pulses, intensity 2.5) and aseptically inoculated (2.5 μl/injection site) using a Hamilton® syringe (Hamilton, NV) unilaterally in the dorsal hippocampus (rate of 0.4 μl/min) and overlying cortex (rate of 0.4 μl/min) (Bregma: −2.54 mm; lateral: +2 mm; depth: − 2.4 mm and −1.4 mm, respectively, from the top of the skull) (Figure 5A).

Mouse tissue collection

Mice were lethally anaesthetised using ketamine/xylazine/acepromazine, and intracardially perfused first with cold DPBS and then perfused-fixed with 20 ml of 10% neutral-buffered formalin (NBF) (rate = 2 ml/min). The brains were dissected and post-fixed in NBF overnight at 4°C. Fixed brains were rinsed in leaching buffer (50 mM Tris, 150 mM NaCl, pH 8.0), cut in 2-mm-thick coronal slices, and processed for paraffin embedding.

Immunocytochemistry

iGFP-NLSm cells were fixed with 4% paraformaldehyde (PFA) in PBS When indicated, to remove cytoplasmic soluble proteins and visualise the insoluble TDP-43 aggregates cells were fixed in 4% PFA containing 1% Triton X-100 for 15 min to remove soluble proteins and processed as described in Porta et al.[20] Cells were incubated with specific primary antibodies overnight at 4°C followed by incubation with secondary antibodies for 1 h at room temperature (Table S4). Coverslips were mounted with Fluoromount G™ containing DAPI (Thermo Scientific Inc., Rockford, IL).

The presence of p409–410-positive aggregates and its classification (%) as spherical, wisp/skein-like aggregates or both was evaluated in three biological replicates by manually counting cells using the ImageJ software. In each replicate, ten different images were obtained at 40x magnification in a high-resolution Leica DMI6000B microscope. An average of 408 ± 139 cells was counted for each time point analysed. All the quantifications were performed blinded with respect to the patient-derived extracts used for transduction.

The values of circularity ($4\pi \times \text{area}/(\text{perimeter})^2$) and roundness ($4 \times \text{area}/(\pi \times (\text{major\_axis})^2)$) of the silhouettes of p409–410-positive aggregates were measured using the ImageJ software (Fiji).[34] For the analysis, ten different 40x images were used for each FTLD-TDP subtype. Immunofluorescent images were converted to digital binary images and the values of circularity and roundness of aggregate-size class were integrated into a total circularity and roundness distribution for the individual samples. The calculated frequency distributions of circularity and roundness data, ranging from 0 to 1.0 with 0.05 intervals were generated with Prism software 7.0 (GraphPad Software, La Jolla, CA).

Immunohistochemistry

IHC studies were performed in paraffin-embedded coronal mouse brain (6 μm) as described in Porta et al.[20] Briefly, deparaffinised and rehydrated. brain sections were blocked and immunostained with the corresponding primary antibody (Table S4) overnight at 4°C.

Sections were incubated for 1 h at room temperature with a biotin-conjugated secondary antibody (Table S4). Antigen-antibody reactions were visualised using VECTASTAIN AB solution and ImmPACT DAB solution (Vector Laboratories Inc., Burlingame, CA) and counterstained with haematoxylin solution. Bright-field images were acquired at 20x magnification using a Lamina Multilabel slide scanner (Perkin Elmer, Waltham, MA).

For double-label immunofluorescence, deparaffinised sections were blocked and incubated with different combinations of primary antibodies overnight at 4°C (Table S4). Secondary antibodies (Table S4) were incubated for 2 h at room temperature in a humidified chamber. To reduce endogenous autofluorescence, brain sections were immersed in a 0.3% Sudan black-70% ethanol solution for 15–20 seconds, followed by a wash in water for 10 min. Finally, sections were mounted in Vectashield-hard medium containing DAPI (Vector Laboratories Inc., Burlingame, CA). Images were obtained in a high-resolution Leica DMI6000B microscope using the Leica LAS-X software.

Immunoblot analyses

The biochemical analyses of sark-insoluble TDP-43 proteins from human FTLD-TDP brains (~1–4 ng TDP-43 protein/lane) or iGFP-NLSm transduced cells (1/3 of sark-insoluble fraction) were analysed on 12% Bis–Tris gels (NuPAGE Novex, Thermo Scientific Inc., Rockford, IL) as described in Porta et al.[20] Membranes were immunoblotted overnight at 4°C with primary antibodies (Table S4). After three washes in 0.1 M Tris buffer with 0.1% Tween-20 membranes were incubated with IRDye-labelled secondary antibodies (Table S4). Blots were scanned using an Odyssey infrared system (ODY-2816 Imager) and the images analysed with the Image Studio software (LI-COR Biotechnology, Lincoln, NE).

PK digestion assay

For PK digestion, ~7 μg of total protein from brain-derived sark-insoluble extracts (~ 1.0–4.0 ng of TDP-43 protein (Elisa C89)) was incubated with increasing concentrations of PK (i.e. 0, 0.25, 0.5, 1.0, 2.5 μg/ml) for 30 min at 37°C.[20] The reaction was stopped with 5 mM PMSF and samples were centrifuged at 100,000xg for 1 h at 4°C. The pellet was resuspended in 20 μl of 1x Laemmli buffer and analysed by immunoblot.

Electron microscopy

Transmission EM images were collected using a JEOL-1010 electron microscope at the University of Pennsylvania Biomedical Imaging Core. Immuno-EM of iGFP-NLSm cells transduced with brain-derived FTLD-TDP extracts was performed as previously described[35] using mAb p409–410 as the primary antibody.

Statistics

For each analysis, the corresponding statistics test is indicated in the figure legend. Statistical analysis of cytotoxicity and viability assays was performed using one-way analysis of variance (ANOVA) using Prism software 7.0 (GraphPad Software, La Jolla, CA). The statistical analysis of the cumulative distribution of roundness and circularity values was performed using the Kolmogorov–Smirnov unpaired *t*-test (p-value < 0.0001) Statistical

analysis of PK resistance assay was performed using a linear mixed-effects model using R studio 3.0.1+.

RESULTS

Morphological differences in TDP-43 aggregates in GFP-NLSm expressing cells seeded with brain-derived TDP-43 extracts from distinct FTLD-TDP subtypes

We and others have shown that brain-derived pathological TDP-43 protein extracted from FTLD-TDP cases act as pathogenic seeds to form *de novo* TDP-43 aggregates in a recipient cell by corrupting the normal protein to adopt pathological conformations *in vitro*.[20,21,24,25] Here, we evaluated whether brain-derived TDP-43 protein obtained from FTLD-TDP cases characterised by four of the five known TDP-43 subtypes A, B, C and E, have distinct seeding properties. Type D was not included here due to our lack of frozen brain samples. The iGFP-NLSm stable cell line generated previously[20] was used as a cell-based reporting system to evaluate the morphology of TDP-43 aggregates induced by distinct TDP-43 pathogenic seeds (Figure S1A and Table S1). Equivalent amounts of brain-derived pathological TDP-43 proteins (sark-insoluble fraction) were transduced in iGFP-NLSm cells (Figure S1B and Table S2) and three days-post transduction (dpt) triton-insoluble and phosphorylated TDP-43 aggregates were detected by immunocytochemistry (ICC) using the phospho-specific mAb Ser409/Ser410 (Figure 1A, p409–410, magenta).

In GFP-NLSm expressing cells transduced with either type A and B brain extracts, TDP-43 aggregates were spherical, highly phosphorylated and widely distributed in the cytoplasm (Figure 1A, type A and type B (insets) and Figure S2). p409–410-positive aggregates were not detected when brain-derived pathological TDP-43 from type C cases were used as pathogenic seeds (Figure 1A, type C). In contrast, FTLD-TDP type E seeds resulted in aggregates with a distinctive small linear, straight and wavy fibrillar structure that we called wisps (Figure 1A, type E (inset) and Figure S2) as well as bigger heterogeneous filamentous skein-like aggregates (Figure 1A, type E (arrowhead)). This was confirmed by confocal microscopy using a maximum projection of a Z-stack to visualise the morphological differences between spherical (Figure 1B, type A (arrows) and movie 1) and wisps/skein-like p409–410-positive aggregates (Figure 1B, type E (arrows and arrowheads respectively) and movie 2). The ultra-structure of these spherical (Figure 1C, type A (arrows)) and filamentous (Figure 1C, type E (arrowheads)) aggregates was also analysed by electron microscopy (EM). No significant effects in cytotoxicity (Figure S2B, LDH assay) or viability (Figure S2C, Alamar blue assay) were observed in iGFP-NLSm cells transduced with different FTLD-TDP subtypes when compared with brain-derived extracts from a non-pathological case (CTRL), Bioporter alone or non-transduced condition (Dox+) used as control conditions.

We performed an unbiased morphometric analysis using ImageJ software to evaluate the differences in the shape between spherical and wisps/skein-like TDP-43 aggregates by measuring roundness and circularity parameters (Figure 1D).[34] Posterior analysis of these two parameters showed statistically significant differences in the cumulative distribution of roundness and circularity values of p409–410-positive aggregates for cells transduced with type A vs. type E seeds (Figure 1D, plots). Thus, unbiased analyses of these differently

shaped aggregates provide further support to the hypothesis that the pathogenesis of type A and type E aggregates is distinct.

Time course characterisation for the formation of TDP-43 aggregates and their uniformity

We next characterised the formation of p409–410-positive aggregates over-time in iGFP-NLSm cells transduced with FTLD-TDP brain-derived type A and type E extracts. Triton-insoluble p409–410-positive aggregates were analysed at 1, 2 and 3 dpt (Figure 2A, magenta). Morphological differences between p409–410-positive aggregates in cells transduced with type A vs. type E extracts were detectable as early as 1 dpt. Incipient cytoplasmic spherical aggregates were detected in cells transduced with type A extracts at 1dpt, and the number of these aggregates increased over-time with a concomitant enlargement in the size of these perinuclear aggregates (Figure 2A, top panels (arrows)). In contrast, type E seeds induced both wisps and skein-like aggregates even at 1dpt. Over-time, wisps were still detectable, whereas skein-like aggregates became more prominent and compact (Figure 2A, bottom panels (arrows and arrowheads respectively)).

We evaluated quantitatively the uniformity of the morphological features of TDP-43 aggregates over-time. iGFP-NLSm cells bearing aggregates were classified as either spherical, wisp/skein-like or both (Figure 2B). At the different time points analysed, nearly all the cells transduced with type A extracts bear spherical aggregates (Figure 2B, black bars), whereas cells transduced with type E extracts contain wisp and skein-like aggregates (Figure 2B, grey bars). Since very few cells were found carrying both spherical and wisps/skein-like aggregates in the same cell (Figure 2B, white bars), our data demonstrate a high degree of uniformity in the ability of individual TDP-43 subtypes to induce pTDP-43 inclusions. Overall, these results suggest that distinct TDP-43 strains are present in brain-derived extracts from different FTLD-TDP subtypes and they have specific seeding properties for self-templating TDP-43 protein into aggregates with distinct morphological features.

Morphological features of TDP-43 aggregates induced in iGFP-NLSm cells are propagated from progenitor to offspring cells

We assessed if the TDP-43 aggregates seeded by brain-derived FTLD-TDP extracts could be propagated to daughter cells. Images in Figure S3 show a 12-hour time-frame (i.e. t1-t12) of live imaging of iGFP-NLSm cells transduced with type A (Figure S3A), type B (Figure S3B) and type E (Figure S3C) extracts. Spherical-aggregates in type A and B seeded cells were dynamic and fused as well as unfused rapidly (movie 3 and 4). Prior to cell division, several small aggregates merged to form bigger and elongated aggregates (Figure S3A–B (arrows) and movie 3–4). After cell division, spherical aggregates were detected in daughter cells (Figure S3A (t8) and b (t4) (asterisks)), and these small spherical aggregates evolved over time. In type E seeded cells, wisps and skein-like aggregates were not as dynamic as spherical aggregates (movie 5). However, additional single wisps were recruited into preformed skein-like aggregates over-time (movie 5). After cell division (Figure S3C, t6–t12 (asterisk)), daughter cells showed small cytoplasmic wisps assembled to form a bigger heterogeneous filamentous structure over-time (Figure S3C, t6–t12 (arrow) and movie 5). Unfortunately, to distinguish the wisps aggregates from the diffuse cytoplasmic signal of

GFP-NLSm protein, it was necessary to increase the exposure time of the fluorescence signal during live cell-imaging and consequently, the skein-like structures appeared as bright circular aggregates (Figure S3C, t1–t12 (arrowheads)). These results showed that specific pathological strains appear to be propagated to daughter cells.

Distinct biochemical banding pattern of sark-insoluble TDP-43 proteins recovered from iGFP-NLSm cells transduced with different FTLD-TDP subtypes

Several groups have shown that different biochemically extracted species of pathological TDP-43 have slightly different banding patterns of C-terminal fragments (CTFs).[11,36,37] Immunoblot analysis of the sark-insoluble fractions from FTLD-TDP brains, using a pan-TDP-43 antibody and mAb p409–410, showed the presence of the full-length TDP-43 protein with a Mr of ~43 kDa (Figure S1B, arrowhead) and the characteristic CTFs resulting from partial proteolysis including three major bands with a theoretical Mr ranging between ~20–26 kDa (Figure S1B, bands #1, #2 and #3) and two minor bands at ~18–19 kDa (Figure S1B, bands #4 and #5).[36,37] Although in our patient cohort, the banding pattern of CTFs between type A, B and C extracts was barely indistinguishable as described by other groups, type E extracts exhibited a more prominent CTF band #1 (Figure S1B) when compared with the other previously described TDP-43 subtypes.[11]

To evaluate *in vitro* if the morphological differences in p409–410-positive aggregates were associated with the formation of distinct insoluble TDP-43 species, we analysed the banding patterns of TDP-43 proteins in the sark-insoluble fraction from transduced iGFP-NLSm cells (Figure 3A, left panels). This analysis revealed an accumulation of phosphorylated exogenous GFP-NLSm protein (Figure 3A), endogenous TDP-43 (Figure 3A, arrowhead) and three major C-terminal fragments (Figure 3A, CTFs bands #1, #2 and #3) in cells transduced with type A, B and E extracts (Figure 3A). In contrast, phosphorylated TDP-43 protein was not appreciably recovered from cells transduced with type C extracts, confirming a reduced seeding activity (Figure 3A). No appreciable phosphorylated TDP-43 protein was recovered from cells treated only with transduction reagent (Bioporter) and presence of dox (Figure 3A, right panels, Dox+). A non-phosphorylated N-terminal TDP-43 truncated fragment ~35 kDa is present in all transduction conditions (Figure 3A, left and right panels, asterisk). These results indicated that the accumulation of sark-insoluble and phosphorylated TDP-43 protein present in cells transduced with FTLD-TDP extracts from type A, B and E cases is not just due to the exogenous overexpression of GFP-NLSm protein in presence of dox or due to the transduction reagent.

To confirm that the sark-insoluble full-length TDP-43 proteins and CTFs were newly formed species from transduced GFP-NLSm expressing cells and not from the human brain-derived TDP-43 extracts used as seeds, we first transduced the iGFP-NLSm cells in the absence or presence of dox (Figure 3B, Dox− and Dox + respectively). Next, we analysed the brain-derived extracts used as seeds and the sark-insoluble fraction obtained from cells transduced with the respective brain-derived extracts side-by-side by immunoblotting using a pan-TDP-43 antibody and mAb p409–410 (Figure 3B). There was an increase in insoluble phosphorylated TDP-43 species only in cells expressing exogenously GFP-NLSm protein (Figure 3B, Dox-vs. Dox+). These results demonstrated that insoluble phosphorylated

TDP-43 recovered from GFP-NLSm cells are newly formed TDP-43 species and confirmed that the presence of cytoplasmic TDP-43 enhances the seeding process as described previously.[20] Interestingly, in both the Dox− and Dox + conditions, type E seeds recruited more endogenous TDP-43 proteins into the sark-insoluble aggregates than type A and type B seeds (Figure 3b, arrowhead). In addition, we observed a slightly different banding pattern of intermediate-sized TDP-43 fragments in sark-insoluble extracts from cells transduced with either type A or B vs. type E seeds (Figure 3B, asterisk).

Finally, we carefully compared the banding patterns of CTFs in sark-insoluble extracts from human brains and iGFP-NLSm-transduced cells (Figure 3B, white dashed box, and 3c). A schematic representation of the different CTFs is illustrated in Figure 3C. We detected differences in the biochemical banding patterns of the CTFs in the human brain-derived material (Figure 3C, bands #1, #2 and #3) and sark-insoluble CTFs recovered from transduced cells (Figure 3C, bands #1–6). Curiously, the top CTF product which was more prominent in brain-derived type E extracts (Figure 3C, band #1), appeared as a doublet in the sark-insoluble extracts from the cells transduced with the three different FTLD-TDP subtypes (Figure 3C, bands #1 and #2). The CTF band #3 in the human brain-derived extracts (Figure 3C, band #3) ran slightly different in cell extracts (Figure 3C, Dox+, band #5). Moreover, sark-insoluble extracts from cells transduced with either type A, B or E extracts showed the presence of additional CTFs, including a non-phosphorylated fragment (Figure 3C, Dox+, band #3 (red)) and a fragment with electrophoretic mobility ~20 kDa (Figure 3C, Dox+, band #6). We observed that CTF band #4 was more abundant in sark-insoluble extracts from cells transduced with either type A or B extracts than in type E seeded cells (Figure 3C, Dox+, band #4). The biochemical analysis of the sark-insoluble cells extracts studied here showed the presence of slightly different insoluble TDP-43 products in cells transduced with types A, B vs. type E suggesting that a specific assembly of insoluble TDP-43 in living cells can give rise to distinctive types of TDP-43 aggregates.

Distinct TDP-43 strains present in brain-derived FTLD-TDP extracts are associated with distinctive morphotypes of TDP-43 aggregates *in vitro*

We next evaluated if distinct fragments or conformations of insoluble TDP-43 recovered from FTLD-TDP brains may be responsible for the different TDP-43 morphotypes induced by type A, B and E extracts *in vitro*. We first probed membrane strips containing sark-insoluble fractions from type A and E brains with a panel of different antibodies recognising distinct epitopes across the entire TDP-43 protein including both commercial and in-house made antibodies targeting the mid-domain of TDP-43, the RNA-recognition motive-2 (RRM2) as well as the flanking regions, and the C-terminal low complexity domain (LCD) (Figure S4A). Other than the more abundant top CTF band #1 in type E extracts (Figure S4B, asterisk) that is recognised by several antibodies (i.e. PT#17082, 2E2-D3, 2052, c2089 and p409–410), the analysis did not reveal TDP-43 fragments differentially overrepresented that could be interpreted to drive the formation of distinct types of TDP-43 aggregates *in vitro*. However, further study of this is warranted to assess whether more subtle differences can be discerned.

To rule out the possibility that the morphological differences in TDP-43 aggregates observed *in vitro* could be an artefact due to the presence of other contaminants in the brain extracts, we immunoprecipitated TDP-43 proteins from sark-insoluble FTLD-TDP extracts. First, TDP-43 was immunoprecipitated from type A and type E extracts using a rabbit polyclonal C-terminal antibody (C2089). Rabbit IgGs (IgG Rb) were used as a negative control.

Immunodepletion (ID) of TDP-43 proteins from the sark-insoluble fraction was confirmed by immunoblotting with the mAb p409–410 (Figure S4C). Whereas full-length TDP-43 (Figure S4C, arrowhead) and CTFs remained in the extracts incubated with IgG control (Figure S4C, IgG Rb), both were mostly eliminated after incubation with C2089 antibody (Figure S4C, ID TDP43). Next, the immunoprecipitated material was eluted and analysed by immunoblotting (Figure S4D). Notably, immunoprecipitation preserves full-length TDP-43 proteins and the distinctive biochemical signature of the CTFs from the original type A and type E extract (Figure S4C). Finally, immunoprecipitated TDP-43 was used as the pathogenic seeds in iGFP-NLSm cells, and the formation of TDP-43 aggregates was analysed 3 dpt (Figure S4E). It is evident that these aggregates recapitulated the morphological differences observed with the original brain-derived extracts including the formation of spherical aggregates (Figure S4C, arrows) in cells transduced with immunoprecipitated TDP-43 proteins from type A extracts, and the formation of wisps (Figure S4E, arrows) and skein-like aggregates (Figure S4E, arrowhead) in cells transduced with immunoprecipitated TDP-43 from type E extracts. These results support the idea that specific TDP-43 strains are present in extracts from different FTLD-TDP subtypes and contaminating proteins do not result in defined seeding properties.

To further explore whether the distinct morphologies of TDP-43 aggregates induced *in vitro* were due to distinct TDP-43 strains, we assessed the conformational differences in pathological TDP-43 protein present in FTLD-TDP brains using a proteinase K (PK) digestion assay.[19,20,25,38,39] The relative resistance of TDP-43 protein to PK digestion was evaluated using increasing concentrations of PK and analysed by immunoblotting (Figure 4A). The percent of PK resistance of full-length TDP-43 protein (Figure 4A, arrowhead) and each major CTF (Figure 4A, CTFs bands #1–5) was quantified and plotted as a function of the PK concentration, normalising in each case the signal to PK non-digested products (Figure 4B). A linear mixed-effects model demonstrated that full-length TDP-43 protein (Figure 4C, TDP-43) and the CTF band #1 (Figure 4C) exhibited a significant higher susceptibility to PK digestion in type E extracts relative to type A and B extracts (Figure 4C, full length TDP-43 $p = 0.025$; CTF band #1 $p = 0.023$). The steeper decline in % PK resistance of TDP-43 FL and CTF band #1 suggests the presence of distinct brain-derived TDP-43 strains in type E cases vs. type A/B cases which could convey different pathological properties on these proteins that are reflected as a difference in disease mechanism.

Brain-derived TDP-43 strains from FTLD-TDP subtypes display distinct seeding properties *in vivo*

We recently showed that injections of sark-insoluble extracts from FTLD-TDP type A and B brains into the CNS of TDP-43 Tg as well as WT mice induced the formation of *de novo* phosphorylated TDP-43 aggregates.[20] We also showed that the burden of TDP-43

pathology and its propagation over-time was more abundant when TDP-43 was mislocalised in the cytoplasm of the TDP-43 Tg mice (i.e. CamKIIa-hTDP-43_{NLSm}).[20] Here we used the same Dox-regulatable CamKIIa-hTDP-43_{NLSm} Tg mice to analyse the seeding properties of brain-derived type E extracts and to compare them with previously described results from injections of type A and B extracts *in vivo*.[20] Although type C extracts did not show seeding activity *in vitro*, we tested whether or not type C seeds were capable of inducing *de novo* TDP-43 pathology in mouse brains.

We stereotaxically injected comparable amounts of brain-derived pathological TDP-43 (~1.5 ng TDP-43/injection site) from different FTLD-TDP subtypes (Table S3) into the hippocampus and the overlying cortex (Figure 5A) and evaluated the formation of *de novo* TDP-43 pathology by immunohistochemistry (IHC) using the mAb p409–410 at 1-month post-injection (mpi). We validated the results originally described by Porta et al.,[20] using additional FTLD-TDP type A and type B extracts (Table S3). At 1 mpi, we detected a high burden of p409–410-positive immunostaining in brain areas ipsilateral to the injection (i.e. hippocampus, subiculum, ectorhinal/perirhinal cortex (Ect/PRh) and neocortical areas (cortex)) in the brains of mice injected with type A and B extracts (Figure 5B). However, no p409–410 immunopositive staining was detected in any of the brains of mice injected with type C extracts at 1mpi (Figure 5B), consistent with our cell culture data suggesting that type C strains are poor at seeding TDP-43 protein into aggregates.

Interestingly, the neuropathological analysis of CamKIIa-hTDP-43_{NLSm} brains injected with type E extracts showed a distinctive pattern of p409–410-positive staining when compared with mice injected with type A or type B extracts (Figure 5B, type A or B vs. type E). For example, mice injected with type A or B extracts showed widespread recruitment of TDP-43 protein into p409–410-positive NCIs in CA1 pyramidal cell bodies (Figure 5B, inset (arrows)) and their apical and basal dendrites in the stratum radiatum (rad) and oriens (or) respectively (Figure 5B, (arrowheads)). However, p409–410-positive immunostaining was markedly less abundant in mice injected with type E extracts, and the resulting TDP-43 aggregates showed distinctive morphological characteristics. In the hippocampus of mice injected with type E extracts, p409–410-positive NCIs were restricted to scattered CA1 pyramidal neurons and formed dot-like inclusions (Figure 5B, inset (black arrow)) as well as fibrillar cytoplasmic aggregates (Figure 5B, inset (white arrow)) that resemble skein-like TDP-43 aggregates found in ALS patients. Moreover, scant p409–410-positive immunostaining was detected in neuronal projections in type E injected mice (Figure 5B, *rad* (arrowhead)). These results were confirmed using another TDP-43 phospho-specific antibody that recognises a different TDP-43 phosphorylation-dependent epitope, that is pSer403/pSer404 (Figure S5, p409–410 vs. p403–404).

We used a polyclonal anti-TDP-43 antibody that preferentially recognises hTDP-43 proteins to detect these proteins in mice injected with type A and E brain extracts by IHC (Figure S5, hTDP-43, right panels). Surprisingly, despite the high expression levels of the hTDP-43_{NLSm} protein in the cytoplasm of neurons without aggregates in CamKIIa-hTDP-43_{NLSm} mice (Figure S5, right panels, inset (asterisks)), in both type A and type E injected mice neurons bearing aggregates showed that hTDP-43_{NLSm} proteins were completely recruited into cytoplasmic TDP-43 aggregates (Figure S5, insets (arrows)). Finally, we show that *de novo*

TDP-43 pathology induced in the brain of mice injected with type E was also positive for p62 and ubiquitin (Figure S6) as previously described in mice injected with type A and B extracts.[20]

Differences in morphology and burden of TDP-43 aggregates between CamKIIa-hTDP-43_{NLSm} mice injected with type A or B vs. type E extracts were also detected in other brain regions such as subiculum and Ect/PRh cortex and neocortical areas. The subiculum of type A and B injected mice showed intense p409–410 immunoreactivity in neuronal cell bodies (Figure 5B, insets (black arrow)) and neuropil. In contrast, in type E injected mice, p409–410-positive staining was restricted to scattered neurons, and no staining was observed in the neuropil. Also, as in the hippocampus, cytoplasmic p409–410 aggregates in the subiculum displayed dot-like (Figure 5B, inset (black arrow)) as well as skein-like morphologies (Figure 5B, insets (white arrowheads)). In other brain areas directly interconnected with the hippocampal injection site such as Ect/PRh cortex, mice injected with type A and B extracts consistently showed p409–410-positive NCIs (Figure 5B, insets (black arrowheads)) and neuropil threads in superficial layers contrasting with scarce newly formed p409–410-positive aggregates in mice injected with type E extracts at 1 mpi.

In the ipsilateral cortex, CamKIIa-hTDP-43^{NLSm} mice injected with either type A and type B extracts at 1mpi, showed p409–410-positive NCIs and neuropil threads in different cortical layers, preferentially in layer VI (Figure 5b, layers I-VI and insets (black arrows)) as previously described,[20] whereas only scattered neurons bearing p409–410-positive NCIs are detected in the cortex of mice injected with type E extracts (Figure 5B, layer VI). Moreover, in contrast with the wide distribution of pTDP-43 staining in the cytoplasm and proximal projections in type A or B injected mice, TDP-43 pathology in mice injected with type E, displayed perinuclear dot-like aggregates (Figure 5B, inset (black arrow)) and skein-like inclusions (Figure 5B, inset (white arrows)).

Overall, these results confirm that different TDP-43 strains isolated from different FTLD-TDP subtypes have distinct seeding capabilities to self-templating TDP-43 protein into phosphorylated aggregates with a distinctive subcellular distribution and morphology in the brain.

Differences in the spreading pattern of TDP-43 pathology in CamKIIa-hTDP-43_{NLSm} Tg mice injected with pathological TDP-43 strains from different FTLD-TDP subtypes

We recently showed that in the brains of mice injected with brain-derived insoluble TDP-43 (e.g. type A and type B), the TDP-43 pathology propagated and spread in the brain in a time-dependent manner to distal areas from the injections site, including the contralateral side as well as to rostral and caudal brain areas distal to the injection site.[20]

We describe here notable TDP-43 aggregate seeding and propagation differences over time between brain-derived TDP-43 obtained from different FTLD-TDP subtypes in the brains of CamKIIa-hTDP-43_{NLSm} mice. We evaluated how the differences in seeding affected the propagation and spreading of TDP-43 pathology throughout the brain over-time at 3 mpi. As previously described,[20] we confirmed an increase in the burden and wide spreading of TDP-43 pathology to rostral and caudal brain areas distal to the injection site (Figure 6A)

using additional type A and B extracts injected into CamKIIa-hTDP-43$_{NLSm}$ mice at 3 mpi (Figure 6B and Figure S7). These results contrasted with the absence of p409–410-positive staining in mice injected with type C seeds (Figure 6B, and Figure S7) and the limited spreading of TDP-43 pathology in brains of CamKIIa-hTDP-43$_{NLSm}$ mice injected with type E seeds in both ipsilateral (Figure 6B) and contralateral side of the brain (Figure S6). The spreading pattern of TDP-43 pathology in the brains of mice injected with type E extracts was mainly restricted to specific brain areas in the ipsilateral side such as the caudal hippocampus and subiculum (Figure 6B), the parahippocampal region (PHR) and lateral entorhinal cortex (Figure 6B, LEnt) and the ventral retrosplenial cortex (Figure 6B, RSCv).

In addition to differences in the burden and limited spreading of TDP-43 pathology, differences in the morphology and subcellular distribution of TDP-43 aggregates were also visible at 3 mpi compared with the brains of mice injected with type E vs. type A or B extracts. Mice injected with type A or type B extracts, showed a higher burden of p409–410-positive NCIs (Figure 6B and insets (arrow)), short and long DNs (Figure 6B, black arrowheads) as well as dot-like staining in the neuropil (Figure 6B, white arrowheads). We also noted the presence of p409–410-positive staining in white matter tracts in the dorsal hippocampal commissure adjacent to the subiculum (caudal) (Figure 6B, dhc, white arrowheads). In contrast, CamKIIa-hTDP-43$_{NLSm}$ mice injected with type E extracts developed TDP-43 pathology only in scattered neurons with p409–410-positive NCIs showing perinuclear dot-like and skein-like morphologies (Figure 6B, black and white arrows respectively (insets)). Furthermore, we also detected an increase in dot-like staining in the (Figure 6B, white arrowheads) in the subiculum of the caudal subiculum and RSCv. Notably, in mice injected with type A and B extracts, the TDP-43 pathology spreads to additional cortical areas such as the visual cortex (Figure 6B, VIS) and ventral (Figure 6B, RSCv) and lateral agranular retrosplenial cortex (Figure 6B, RSCagl). In contrast, in type E injected Tg mice, TDP-43 pathology was found mainly in the RSCv. Moreover, the spreading of TDP-43 pathology was not detected in the contralateral side of the brain in mice injected with type E extracts. Only one of ten injected mice showed a few cells with p409–410-positive dot-like NCIs in the contralateral hippocampus (Figure S7, inset (arrow)).

The burden of TDP-43 pathology in cortical and hippocampal brain areas in mice injected with FTLD-TDP type A, B and E extracts was quantified at 1 and 3 mpi and represented as heat-maps to visualise the spreading pattern throughout the brain (Figure S8). The heat-maps showed some differences in the burden of TDP-43 pathology between mice injected with brain-derived type A and B seeds, however, the spreading pattern in the ipsilateral (Figure S8, ipsi) and contralateral (Figure S8, contra) sides and in rostral (Figure S8, Bregma - 2.3 mm) and caudal brain areas (Figure S8, Bregma – 3.52 mm and −4.48 mm) distal from the injection site (Figure 5A, Bregma – 2.54 mm) is similar over-time. In contrast, TDP-43 pathology in mice injected with type E extracts, as described above, is very restricted to brain areas such as CA1 layer, subiculum and in some brain regions, the small burden of TDP-43 pathology was not distinguishable from the background. The burden of TDP-43 pathology in each region analysed and for each individual injected mouse is represented in the colour-scale plots at 1 and 3 mpi (Figure S8, right panels).

We analysed an additional time-point at 9 mpi for CamKIIa-hTDP-43_{NLSm} mice injected with type C and E extracts. Even at longer time points, no p409–410 immunostaining was detected in the brains of mice injected with type C TDP-43 pathology and in only one of five mice injected we identified a few p409–410-positive NCIs (Figure S9A, insets) and DNs (Figure S9A, black arrowheads) in the ipsilateral hippocampus and subiculum. At 9 mpi, there was no increase in the burden of p409–410-positive NCIs or spreading of TDP-43 pathology to other brain areas in the CamKIIa-hTDP-43_{NLSm} mice injected with type E extracts. The same ipsilateral brain areas affected at 3 mpi (i.e. the RSCv and sub, and white matter tracts in the dhc) showed p409–410-positive neuritic threads (Figure S9A, black arrowheads), cytoplasmic inclusions (Figure S9A, inset) and dot-like pathology in the neuropil (Figure S9A, white arrowheads).

The presence of TDP-43 pathology in glial cells at later time-points (i.e. 9 mpi) was a characteristic feature reported in the brains of CamKIIa-hTDP-43_{NLSm} mice injected with type A and B extracts.[20] Here we also detected the formation of p409–410-positive inclusions in oligodendrocytes (Figure S9B, olig2, arrows), whereas p409–410-positive inclusions were largely not associated with Sox9-positive cells used as an astrocytic marker (Figure S9B, arrowheads).

DISCUSSION

The specific neuroanatomical distribution and morphological features of TDP-43 pathology found in autopsy brains from FTLD-TDP patients define distinct subtypes (type A-E) associated with different clinical manifestations of disease and unique genetic contributions.[2–10] Little is known about the underlying mechanisms that could explain the characteristic patterns of misfolded and mislocalised TDP-43 protein across specific brain regions and their distinct clinicopathological phenotypes. *In vitro* evidence indicates that different conformational forms of TDP-43 protein referred to as strains and recovered biochemically from the brains of patients who manifest different FTLD-TDP neuropathological subtypes have distinct seeding activities and toxic properties in cell culture.[20,23,25,40] However, a major gap in our understanding is whether or not different TDP-43 strains contribute to the phenotypic heterogeneity of TDP-43 pathology in the brains of FTLD-TDP patients.

In this study, we provide evidence that distinct brain-derived TDP-43 strains from different FTLD-TDP subtypes self-template TDP-43 protein into aggregates with specific morphological features or morphotypes *in vitro*. Furthermore, we show that intracerebral injections of brain-derived TDP-43 strains from FTLD-TDP brains into Tg mice expressing cytoplasmic human TDP-43 induce a distinctive morphological and subcellular distribution of TDP-43 pathology as well different spreading patterns in the brain.

Despite the differences in distribution and neuropathological features of TDP-43 pathology that characterise FTLD-TDP type A and type B subtypes, similar cytoplasmic spherical TDP-43 aggregates are induced in GFP-NLSm expressing cells when sark-insoluble TDP-43 protein derived from the frontal cortex of these subtypes are used as pathogenic seeds. The spherical shape of these aggregates contrasts with the linear and wavy wisps, and skein-like

structures formed when brain-derived TDP-43 from type E cases are used as pathogenic seeds. Spherical aggregates induced in iGFP-NLSm cells may resemble the round and compact cytoplasmic inclusions detected in the brains of type A and B cases. In contrast, wisps and skein-like structures bear some resemblance to TDP-43 skeins observed in motor neurons in ALS and the cytoplasmic diffuse and granulofilamentous neuronal inclusions (GFNIs) characteristic in FTLD-TDP type E brains. The significance of these morphological differences on the pathological behaviour of these subtypes remains to be elucidated.

Interestingly, TDP-43 aggregates with both spherical and wisps/skein-like morphologies were not observed in the same or adjacent iGFP-NLSm cells transduced with FTLD-TDP extracts. These results contrast with the diversity of morphological presentations of TDP-43 aggregates described by Smethurst et al.[22] in cells overexpressing WT TDP-43 transduced with seeds isolated from the post-mortem brains of amyotrophic lateral sclerosis (ALS) patients.[22] The coexistence of wisps, skein-like aggregates, dot-like and round TDP-43 aggregates found in motor neurons of deceased ALS patients could explain the differences in the homogeneity of TDP-43 morphotypes induced with ALS and FTLD-TDP pathogenic seeds *in vitro* as well as differences in mechanisms of disease pathogenesis.[22]

The formation of distinct phosphorylated TDP-43 morphotypes in GFP-NLSm expressing cells seeded with extracts from different FTLD-TDP subtypes correlates biochemically with the presence of specific sark-insoluble N-terminal truncated fragments of TDP-43 protein. Differences in N-terminal sequences with similar C-terminal aggregation-prone fragments of TDP-43 have been shown to have a profound influence on fragment metabolism, propensity to form insoluble aggregates, as well as aggregate morphology [41] all of which could impact disease mechanism. Kasu et al.[41] described that N-terminal truncated TDP-43; $TDP_{219–414}$ and $TDP_{247–414}$, despite being ~85% similar, when overexpressed in HEK293 T cells formed morphologically distinct intracellular aggregates.[41] Although some studies have shown a distinctive band pattern of CTFs when comparing type A, B and C brain extracts,[11,36,37] these differences are not noticeable when we compare the band pattern of TDP-43 CTFs of our sark-insoluble extracts. We hypothesise that different biochemical fractionation conditions, including distinct solubilisation of the final sark-insoluble material, and variations of electrophoretic conditions could modify the mobility of TDP-43 truncated products explaining the discrepancies between studies.

Based on epitope mapping experiments using a panel of antibodies against TDP-43 proteins, we confirm that an N-terminal truncated TDP-43 fragment with lower electrophoretic mobility (CTF band #1) containing amino acids residues ~203–209 is overrepresented in type E extracts as described by Lee et al.[11] These findings support the hypothesis that a critical concentration of CTFs could determine the formation of specific spherical or filamentous TDP-43 aggregates, as indicated by Kasu et al.[41]

We also show that specific immunoprecipitated TDP-43 protein from brain-derived sark-insoluble extracts when transduced into iGFP-NLSm cells, recapitulates the differences in morphology of *de novo* seeded TDP-43 aggregates. Although we cannot completely rule out the contribution of other sark-insoluble proteins co-aggregating with TDP-43 as described recently by Laferrière et al.,[23] our data indicate that TDP-43 protein plays a significant role

in the formation of distinct TDP-43 morphotypes. In addition, the differential susceptibility to PK digestion of type E extracts also supports the role of TDP-43 conformational differences associated with the formation of morphological distinctive TDP-43 aggregates between FTLD-TDP subtypes.

Regarding the morphological features and spreading patterns of TDP-43 pathology, no noticeable differences were found in the brain of CamKIIa-hTDP-43$_{NLSm}$ mice injected with either type A or B extracts. Here, we confirm these results using additional FTLD-TDP brain extracts not tested previously in Porta et al.[20] Furthermore, we show a distinctive morphology and subcellular distribution of TDP-43 aggregates induced in the brain of CamKIIa-hTDP43$_{NLSm}$ mice injected with TDP-43 type A and B strains vs. type E. Interestingly, pTDP-43 aggregates induced by type A and B extracts resemble the dense, and compact NCIs described in human FTLD-TDP brains belonging to the same subtype. On the other hand, TDP-43 strains from type E extracts induced dot-like perinuclear inclusions and skein-like aggregates that resembled the type of pathology found in motor neurons of patients with FTLD-MND and ALS[1,2,42–47] than the characteristic GFNIs of FTLD-TDP type E cases.[11] In addition to differences in morphology, the presence of TDP-43 pathology in the soma but also in neuronal projections in mice injected with type A and B extracts, contrasts with mainly perinuclear TDP-43 pathology in type E injected mice. These differences in subcellular distribution of TDP-43 pathology could determine a distinctive toxic effect of both type A and B strains in injected mice by affecting the neuronal function as a consequence of a potential disruption in axonal and/or dendritic transport.

We observed that brain-derived TDP-43 extracts from type C cases exhibited no remarkable seeding activity *in vivo*, including at 9 mpi. These results validate our *in vitro* data and previously published data indicating that among the different FTLD-TDP subtypes analysed, type C represents the less potent TDP-43 strain self-templating TDP-43 protein into aggregates.[23,25] Recently, it has been shown the association of type C Sarko-spin fraction to very dense TDP-43 aggregates, the lesser extent of polyubiquitination, and a highly protease-resistant C-terminal core, when compared with type A sark-insoluble TDP-43 aggregates.[23] Interestingly, FTLD-TDP type E cases are associated with rapidly progressive frontotemporal degeneration.[11]

The present study based on post-mortem brain samples captures the end-stage of the diseased brains. However, it remains unknown if a mixture of TDP-43 strains may be originated at the beginning of the disease, and distinct cellular vulnerability, cellular milieu, together with genetic and/or environmental factors may determine that specific strains evolve and propagate during the disease course, potentially determining certain disease phenotypes. Further studies are needed to elucidate if the maturation state of TDP-43 aggregates including; differences in compaction, post-translational modifications such as phosphorylation, acetylation, ubiquitination, as well as proteolytic fragmentation among other variables such as disease duration may be determining factors that govern the distinct seeding properties of the different TDP-43 strains.

In addition to the different morphology of TDP-43 aggregates, we found a remarkable difference in the spreading efficiency of TDP-43 pathology over-time. In mice

stereotaxically injected with either type A or B extracts, TDP-43 pathology progressively spreads in a time-dependent manner throughout the brain. In contrast, in type E injected mice, the spreading is restricted to brain areas interconnected with the injection site. The differences in subcellular distribution of TDP-43 pathology may determine the efficiency of transmission of pathogenic species, the capacity of spreading and consequently the degree of pathogenicity. The notable p409–410 immunoreactivity in the stratum radiatum and oriens in the hippocampus proper of mice injected with type A and type B extracts, as well as in white matter tracts, including the corpus callosum, ventral hippocampal commissure, among other regions described by our group[30] is consistent with the hypothesis that pathological TDP-43 species propagate via axonal connections. In rodents, the ventral hippocampal commissure supports dense interhemispheric connections between the hippocampi,[48,49] consistent with the potential spreading of TDP-43 pathology to contralateral brain areas through these tracts in mice injected with type A and type B extracts. On the other hand, in the brains of mice injected with type E extracts, dot-like and skein-like p409–410-positive aggregates are mainly perinuclear. Moreover, no p409–410 immunoreactivity was found in white matter tracts except the dorsal hippocampal commissure, proximal to the subicular regions. In non-human primates the dorsal hippocampal commissure carries projections to and from the PHR, including the presubiculum, parasubiculum and entorhinal cortex.[50] Consistent with the spreading of TDP-43 pathology through commissural projections, mice injected with type E extracts show p409–410-positive staining in these three PHR brain areas in a time-dependent manner. Furthermore, PHR receives inputs from CA1 and subiculum,[51–53] brain areas already bearing TDP-43 pathology at the earliest time point of 1 mpi. Moreover, in these mice, TDP-43 pathology also spreads to RSCv, reciprocally connected with PHR brain areas,[54] and that also receives direct input from CA1 and subiculum[51,55,56] supporting an anterograde and retrograde transport of pathological TDP-43 species.

Although our experimental animal model does not fully recapitulate the characteristic neuropathological distribution and spreading patterns of TDP-43 pathology found in the brains of each of the human FTLD-TDP subtypes, we demonstrate here that distinct TDP-43 strains present in brain extracts from different FTLD-TDP subtypes induce distinct morphological types of TDP-43 aggregates as well as distinct spreading patterns in the brain of CamKIIa-hTDP-43$_{NLSm}$ mice. Our experimental data support the hypothesis that distinct TDP-43 strains may contribute to phenotypic heterogeneity of TDP-43 pathology through different mechanisms of disease pathogenicity in the brains of FTLD-TDP cases.

Supplementary Material

Refer to Web version on PubMed Central for supplementary material.

ACKNOWLEDGEMENTS

The authors specially thank the patients and their families for enabling this research conducted here. We also thank C. Lee, M. Dominique, C. Webb for technical assistance and maintenance of the mouse colony; S. Sariol for helping with tissue sectioning; T. Schuck, J. Robinson and B. Alfaro for assistance with obtaining suitable brains for these studies; Dr V. Van Deerlin and Dr E. Suh for the genetic analysis; Dr Michael X. Henderson for guidance with heat-map analysis and S. Leight for administrative support. We thank Manuela Neumann and Elisabeth Kremmer for providing the phosphorylation-specific TDP-43 antibody TAR5P-1D3.

Funding information

This work was supported by NIH grants P30 AG10124, PO1 AG17586, U19 AG062418, the Wyncote Foundation and a research grant from AC Immune SA.

DATA AVAILABILITY STATEMENT

All relevant data are available from the corresponding author upon reasonable request.

REFERENCES

1. Neumann M, Sampathu DM, Kwong LK, et al. Ubiquitinated TDP-43 in frontotemporal lobar degeneration and amyotrophic lateral sclerosis. Science. 2006;314(5796):130–133. [PubMed: 17023659]
2. Cairns NJ, Neumann M, Bigio EH, et al. TDP-43 in familial and sporadic frontotemporal lobar degeneration with ubiquitin inclusions. Am J Pathol. 2007;171(1):227–240. [PubMed: 17591968]
3. Forman MS, Mackenzie IR, Cairns NJ, et al. Novel ubiquitin neuropathology in frontotemporal dementia with valosin-containing protein gene mutations. J Neuropathol Exp Neurol. 2006;65(6):571–581. [PubMed: 16783167]
4. Geser F, Martinez-Lage M, Robinson J, et al. Clinical and pathological continuum of multisystem TDP-43 proteinopathies. Arch Neurol. 2009;66(2):180–189. [PubMed: 19204154]
5. Josephs KA, Stroh A, Dugger B, Dickson DW. Evaluation of subcortical pathology and clinical correlations in FTLD-U subtypes. Acta Neuropathol. 2009;118(3):349–358. [PubMed: 19455346]
6. Mackenzie IR, Baborie A, Pickering-Brown S, et al. Heterogeneity of ubiquitin pathology in frontotemporal lobar degeneration: classification and relation to clinical phenotype. Acta Neuropathol. 2006;112(5):539–549. [PubMed: 17021754]
7. Mackenzie IR, Neumann M. Reappraisal of TDP-43 pathology in FTLD-U subtypes. Acta Neuropathol. 2017;134(1):79–96. [PubMed: 28466142]
8. Mackenzie IR, Neumann M, Baborie A, et al. A harmonized classification system for FTLD-TDP pathology. Acta Neuropathol. 2011;122(1):111–113. [PubMed: 21644037]
9. Neumann M, Mackenzie IR, Cairns NJ, et al. TDP-43 in the ubiquitin pathology of frontotemporal dementia with VCP gene mutations. J Neuropathol Exp Neurol. 2007;66(2):152–157. [PubMed: 17279000]
10. Sampathu DM, Neumann M, Kwong LK, et al. Pathological heterogeneity of frontotemporal lobar degeneration with ubiquitin-positive inclusions delineated by ubiquitin immunohistochemistry and novel monoclonal antibodies. Am J Pathol. 2006;169(4):1343–1352. [PubMed: 17003490]
11. Lee EB, Porta S, Michael Baer G, et al. Expansion of the classification of FTLD-TDP: distinct pathology associated with rapidly progressive frontotemporal degeneration. Acta Neuropathol. 2017;134(1):65–78. [PubMed: 28130640]
12. Goedert M, Falcon B, Clavaguera F, Tolnay M. Prion-like mechanisms in the pathogenesis of tauopathies and synucleinopathies. Curr Neurol Neurosci Rep. 2014;14(11):495. [PubMed: 25218483]
13. Luk KC, Kehm V, Carroll J, et al. Pathological alpha-synuclein transmission initiates Parkinson-like neurodegeneration in nontransgenic mice. Science. 2012;338(6109):949–953. [PubMed: 23161999]
14. Prusiner SB, Woerman AL, Mordes DA, et al. Evidence for alpha-synuclein prions causing multiple system atrophy in humans with parkinsonism. Proc Natl Acad Sci U S A. 2015;112(38):E5308–E5317. [PubMed: 26324905]
15. Heilbronner G, Eisele YS, Langer F, et al. Seeded strain-like transmission of beta-amyloid morphotypes in APP transgenic mice. EMBO Rep. 2013;14(11):1017–1022. [PubMed: 23999102]
16. Petkova AT, Leapman RD, Guo Z, Yau WM, Mattson MP, Tycko R. Self-propagating, molecular-level polymorphism in Alzheimer's beta-amyloid fibrils. Science. 2005;307(5707):262–265. [PubMed: 15653506]

17. Hasegawa M Molecular mechanisms in the pathogenesis of alzheimer's disease and tauopathies-prion-like seeded aggregation and phosphorylation. Biomolecules. 2016;6(2).
18. He Z, Guo JL, McBride JD, et al. Amyloid-beta plaques enhance Alzheimer's brain tau-seeded pathologies by facilitating neuritic plaque tau aggregation. Nat Med. 2018;24(1):29–38. [PubMed: 29200205]
19. Narasimhan S, Guo JL, Changolkar L, et al. Pathological tau strains from human brains recapitulate the diversity of tauopathies in nontransgenic mouse brain. J Neurosci. 2017;37(47):11406–11423. [PubMed: 29054878]
20. Porta S, Xu Y, Restrepo CR, et al. Patient-derived frontotemporal lobar degeneration brain extracts induce formation and spreading of TDP-43 pathology in vivo. Nat Commun. 2018;9(1):4220–4235. [PubMed: 30310141]
21. Shimonaka S, Nonaka T, Suzuki G, Hisanaga S, Hasegawa M. Templated aggregation of TAR DNA-binding protein of 43 kDa (TDP-43) by seeding with TDP-43 peptide fibrils. J Biol Chem. 2016;291(17):8896–8907. [PubMed: 26887947]
22. Smethurst P, Newcombe J, Troakes C, et al. In vitro prion-like behaviour of TDP-43 in ALS. Neurobiol Dis. 2016;96:236–247. [PubMed: 27590623]
23. Laferrière F, Maniecka Z, Perez-Berlanga M, et al. TDP-43 extracted from frontotemporal lobar degeneration subject brains displays distinct aggregate assemblies and neurotoxic effects reflecting disease progression rates. Nat Neurosci. 2019;22(1):65–77. [PubMed: 30559480]
24. Feiler MS, Strobel B, Freischmidt A, et al. TDP-43 is intercellularly transmitted across axon terminals. J Cell Biol. 2015;211(4):897–911. [PubMed: 26598621]
25. Nonaka T, Masuda-Suzukake M, Arai T, et al. Prion-like properties of pathological TDP-43 aggregates from diseased brains. Cell Rep. 2013;4(1):124–134. [PubMed: 23831027]
26. Igaz LM, Kwong LK, Lee EB, et al. Dysregulation of the ALS-associated gene TDP-43 leads to neuronal death and degeneration in mice. J Clin Invest. 2011;121(2):726–738. [PubMed: 21206091]
27. Walker AK, Spiller KJ, Ge G, et al. Functional recovery in new mouse models of ALS/FTLD after clearance of pathological cytoplasmic TDP-43. Acta Neuropathol. 2015a;130(5):643–660. [PubMed: 26197969]
28. Walker AK, Tripathy K, Restrepo CR, et al. An insoluble frontotemporal lobar degeneration-associated TDP-43 C-terminal fragment causes neurodegeneration and hippocampus pathology in transgenic mice. Hum Mol Genet. 2015b;24(25):7241–7254. [PubMed: 26476406]
29. Toledo JB, Van Deerlin VM, Lee EB, et al. A platform for discovery: the university of Pennsylvania integrated neurodegenerative disease biobank. Alzheimers Dement. 2014;10(4):477–484.e1. [PubMed: 23978324]
30. Brettschneider J, Van Deerlin VM, Robinson JL, et al. Pattern of ubiquilin pathology in ALS and FTLD indicates presence of C9ORF72 hexanucleotide expansion. Acta Neuropathol. 2012;123(6):825–839. [PubMed: 22426854]
31. Cirulli ET, Lasseigne BN, Petrovski S, et al. Exome sequencing in amyotrophic lateral sclerosis identifies risk genes and pathways. Science. 2015;347(6229):1436–1441. [PubMed: 25700176]
32. Van Deerlin VM, Gill LH, Farmer JM, Trojanowski JQ, Lee VM. Familial frontotemporal dementia: from gene discovery to clinical molecular diagnostics. Clin Chem. 2003;49(10):1717–1725. [PubMed: 14500612]
33. Paxinos G, Franklin KBJ. The Mouse Brain in Stereotaxic Coordinates, 2nd edn. San Diego: Academic Press; 2001.
34. Schindelin J, Arganda-Carreras I, Frise E, et al. Fiji: an open-source platform for biological-image analysis. Nat Methods. 2012;9(7):676–682. [PubMed: 22743772]
35. Luk KC, Song C, O'Brien P, et al. Exogenous alpha-synuclein fibrils seed the formation of Lewy body-like intracellular inclusions in cultured cells. Proc Natl Acad Sci U S A. 2009;106(47):20051–20056. [PubMed: 19892735]
36. Hasegawa M, Arai T, Nonaka T, et al. Phosphorylated TDP-43 in frontotemporal lobar degeneration and amyotrophic lateral sclerosis. Ann Neurol. 2008;64(1):60–70. [PubMed: 18546284]

37. Hasegawa M, Nonaka T, Tsuji H, et al. Molecular dissection of TDP-43 proteinopathies. J Mol Neurosci. 2011;45(3):480–485. [PubMed: 21678031]
38. Guo JL, Covell DJ, Daniels JP, et al. Distinct alpha-synuclein strains differentially promote tau inclusions in neurons. Cell. 2013;154(1):103–117. [PubMed: 23827677]
39. Peng C, Gathagan RJ, Covell DJ, et al. Cellular milieu imparts distinct pathological alpha-synuclein strains in alpha-synucleinopathies. Nature. 2018;557(7706):558–563. [PubMed: 29743672]
40. Tsuji H, Arai T, Kametani F, et al. Molecular analysis and biochemical classification of TDP-43 proteinopathy. Brain. 2012;135(Pt 11):3380–3391. [PubMed: 23035040]
41. Kasu YAT, Alemu S, Lamari A, Loew N, Brower CS. The N termini of TAR DNA-binding protein 43 (TDP43) C-terminal fragments influence degradation, aggregation propensity, and morphology. Mol Cell Biol. 2018;38(19):e00243–e318. [PubMed: 29987190]
42. Cairns NJ, Bigio EH, Mackenzie IR, et al. Neuropathologic diagnostic and nosologic criteria for frontotemporal lobar degeneration: consensus of the Consortium for Frontotemporal Lobar Degeneration. Acta Neuropathol. 2007;114(1):5–22. [PubMed: 17579875]
43. Davidson Y, Kelley T, Mackenzie IR, et al. Ubiquitinated pathological lesions in frontotemporal lobar degeneration contain the TAR DNA-binding protein, TDP-43. Acta Neuropathol. 2007;113(5):521–533. [PubMed: 17219193]
44. Mackenzie IR, Bigio EH, Ince PG, et al. Pathological TDP-43 distinguishes sporadic amyotrophic lateral sclerosis from amyotrophic lateral sclerosis with SOD1 mutations. Ann Neurol. 2007;61(5):427–434. [PubMed: 17469116]
45. Mori F, Tanji K, Zhang HX, et al. Maturation process of TDP-43-positive neuronal cytoplasmic inclusions in amyotrophic lateral sclerosis with and without dementia. Acta Neuropathol. 2008;116(2):193–203. [PubMed: 18560845]
46. Tan CF, Eguchi H, Tagawa A, et al. TDP-43 immunoreactivity in neuronal inclusions in familial amyotrophic lateral sclerosis with or without SOD1 gene mutation. Acta Neuropathol. 2007;113(5):535–542. [PubMed: 17333220]
47. Zhang H, Tan CF, Mori F, et al. TDP-43-immunoreactive neuronal and glial inclusions in the neostriatum in amyotrophic lateral sclerosis with and without dementia. Acta Neuropathol. 2008;115(1):115–122. [PubMed: 17786458]
48. Demeter S, Rosene DL, Van Hoesen GW. Interhemispheric pathways of the hippocampal formation, presubiculum, and entorhinal and posterior parahippocampal cortices in the rhesus monkey: the structure and organization of the hippocampal commissures. J Comp Neurol. 1985;233(1):30–47. [PubMed: 3980771]
49. Gloor P, Salanova V, Olivier A, Quesney LF. The human dorsal hippocampal commissure. An anatomically identifiable and functional pathway. Brain. 1993;116(Pt 5):1249–1273. [PubMed: 8221057]
50. Boccara CN, Sargolini F, Thoresen VH, et al. Grid cells in pre- and parasubiculum. Nat Neurosci. 2010;13(8):987–994. [PubMed: 20657591]
51. Insausti R, Herrero MT, Witter MP. Entorhinal cortex of the rat: cytoarchitectonic subdivisions and the origin and distribution of cortical efferents. Hippocampus. 1997;7(2):146–183. [PubMed: 9136047]
52. Jones BF, Witter MP. Cingulate cortex projections to the parahippocampal region and hippocampal formation in the rat. Hippocampus. 2007;17(10):957–976. [PubMed: 17598159]
53. Naber PA, Lopes da Silva FH, Witter MP. Reciprocal connections between the entorhinal cortex and hippocampal fields CA1 and the subiculum are in register with the projections from CA1 to the subiculum. Hippocampus. 2001;11(2):99–104. [PubMed: 11345131]
54. Sugar J, Witter MP, van Strien NM, Cappaert NL. The retrosplenial cortex: intrinsic connectivity and connections with the (para) hippocampal region in the rat. An interactive connectome. Front Neuroinform. 2011;5:7. [PubMed: 21847380]
55. Van Groen T, Wyss JM. Extrinsic projections from area CA1 of the rat hippocampus: olfactory, cortical, subcortical, and bilateral hippocampal formation projections. J Comp Neurol. 1990;302(3):515–528. [PubMed: 1702115]

56. Vogt BA, Miller MW. Cortical connections between rat cingulate cortex and visual, motor, and postsubicular cortices. J Comp Neurol. 1983;216(2):192–210. [PubMed: 6863602]

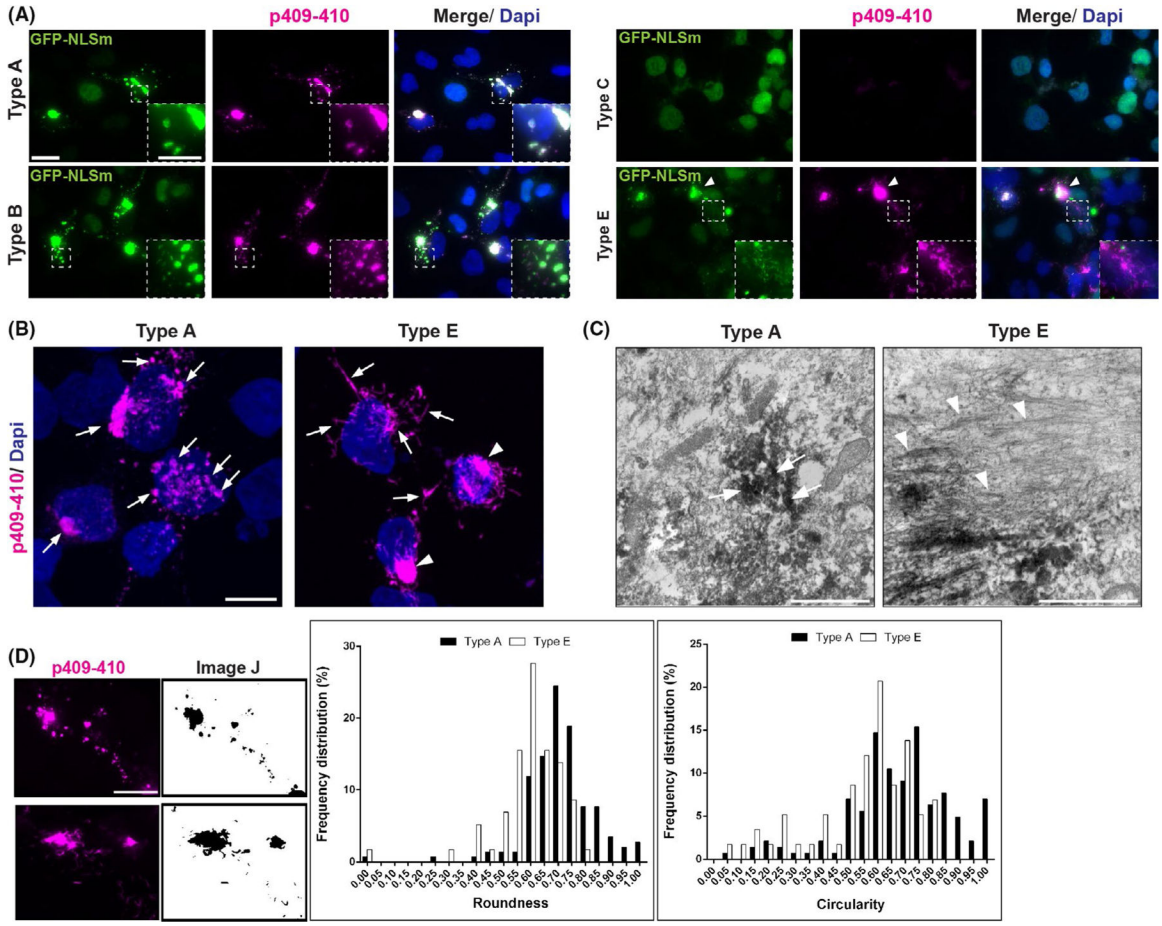

FIGURE 1.

Morphological differences in TDP-43 aggregates in GFP-NLSm expressing cells seeded with brain-derived TDP-43 extracts from distinct FTLD-TDP subtypes. (A) Representative ICC images of GFP-NLSm expressing cells (green and merge) transduced with sark-insoluble brain extracts from different FTLD-TDP subtypes at 3 days post-transduction (dpt) showing 1% Ttriton-insoluble phospho-TDP-43-positive cytoplasmic aggregates (p409–410, magenta and merge). Cells were counterstained with DAPI to label the nuclei (blue). Insets show a magnification of spherical TDP-43 aggregates seeded by type A and type B extracts, and small linear, straight and wavy structures hence wisps seeded by type E extracts. Arrowhead points to heterogeneous filamentous structures hence skein-like aggregates seeded by type E extracts. Scale bar = 20 μm, insets bar = 10 μm. (B) Representative ICC images of a Z-stack maximum projection by confocal microscopy. Arrows point to characteristic p409–410-positive spherical aggregates (magenta) in GFP-NLSm expressing cells transduced with type A. Arrows and arrowheads point to p409–410-positive wisps and skein-like aggregates, respectively, in cells transduced with type E extracts (see also Movies 1 and 2). Cells were counterstained with DAPI to label the nuclei (blue). Scale bar = 10 μm. (C) Immunoelectron microscopy (EM) images show the ultrastructure of p409–410-positive spherical (arrows) and filamentous (arrowheads) aggregates in iGFP-NLSm cells transduced with type A and type E extracts respectively. Note the filaments are most evident where the immunolabelling is faint. Scale bar = 2 μm; insets bar = 1 μm. (D)

Examples of immunofluorescent images (left panels, magenta) converted to digital binary images using ImageJ software (right panels) used to measure the roundness and circularity parameters of the silhouettes of p409–410-positive aggregates at 3dpt. Scale bar = 20 μm. Plots show percentages of the frequency distributions of roundness (left plot) and circularity (right plot) of p409–410-positive aggregates in GFP-NLSm expressing cells transduced with type A (black bars) vs. type E (white bars) extracts at 3 dpt. The calculated roundness and circularity distributions ranged from 0 to 1.0 values with 0.05 intervals. Statistically significant differences in the cumulative distribution of roundness and circularity between p409–410 aggregates in type A vs. type E seeded cells were found using the Kolmogorov–Smirnov unpaired *t*-test ($p < 0.0001$)

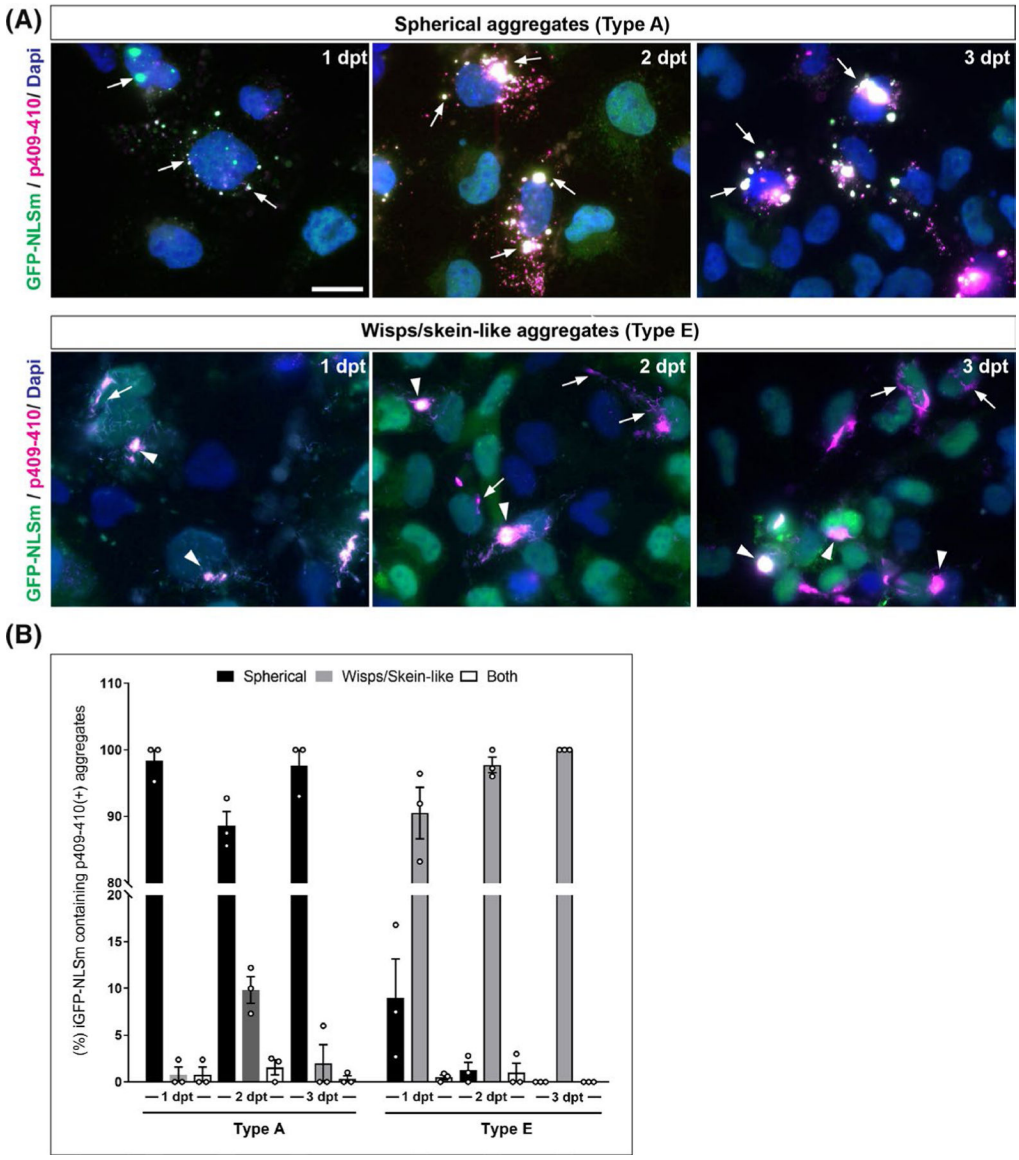

FIGURE 2.

Time course characterisation for the formation of TDP-43 aggregates and their uniformity. (A) Representative ICC images show the formation of cytoplasmic p409–410-positive TDP-43 aggregates (magenta) in GFP-NLSm expressing cells (green) at 1, 2, and 3 dpt. Top panels show characteristic spherical aggregates induced when type A brain extracts are used as seeds (arrows) Bottom panels show characteristics wisps and skein-like aggregates induced by type E seeds (arrows and arrowheads respectively). Cells were counterstained with DAPI to label the nuclei (blue). Scale bar = 20 μm. (B) Plots show the percentages of GFP-NLSm expressing cells bearing p409–410-positive TDP-43 aggregates overtime that are categorised by different morphological features such as spherical (black bars), wisps/skein-like (grey bars) or both (white bars). Bar plots show the mean ± SEM. Each white dot represents a biological replicate ($n = 3$)

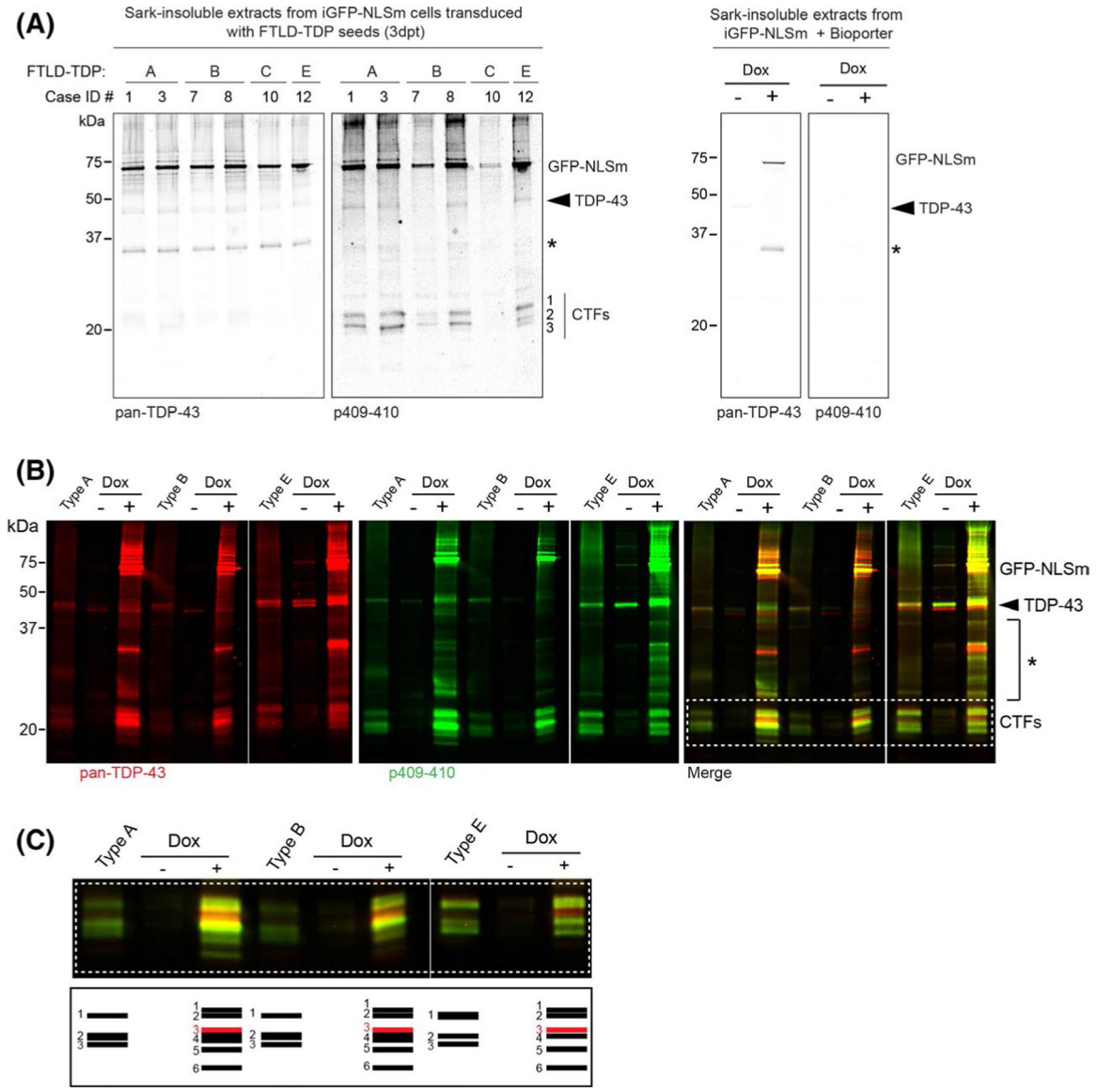

FIGURE 3.

Distinct biochemical banding patterns of sark-insoluble TDP-43 proteins recovered from iGFP-NLSm cells transduced with pathogenic seeds from different FTLD-TDP subtypes. (A) Representative immunoblot analysis of the sark-insoluble fraction from GFP-NLSm expressing cells transduced with different FTLD-TDP subtypes (left panels, type A, B, C and E) and transduction reaction in presence or absence of dox (Dox− and Dox+, Bioporter, right panels). Cases are identified by numbers corresponding to those in Table S1 (Case ID #). A C-terminal TDP-43 antibody was used to detect pan-TDP-43 protein, and the phosphorylation-specific mAb Ser409/Ser410 (p409–410) was used to detect pathological TDP-43. Molecular weight markers in kDa are shown on the left and the position of the GFP-NLSm proteins, endogenous TDP-43 proteins (arrowhead), and three major bands corresponding to C-terminal fragments (CTFs, band #1, #2 and #3) and an N-terminal TDP-43 truncated fragment (asterisk) are shown on the right. (B) Immunoblot analysis of

the sark-insoluble fractions from FTLD-TDP cases used as seeds (lanes type A, B and E) and the corresponding sark-insoluble fraction from the iGFP-NLSm cells transduced in the absence (lanes, Dox −) or presence of doxycycline (lanes Dox +) at 3 dpt. A C-terminal TDP-43 antibody (red and merged with green) was used to detect pan-TDP-43 protein and the p409–410 mAb was used to detect the pathological TDP-43 (green and merged with red). Molecular weight markers in kDa are shown on the left and the positions of the GFP-NLSm protein, endogenous TDP-43 protein (arrowhead, ~43 kDa), intermediate TDP-43 truncated fragments (asterisk), and three major bands corresponding to C-terminal fragments (CTFs) are shown on the right. White dashed box framing the CTF bands is shown for magnification standards in C (top panel). The schematic diagram in c (bottom panel) illustrates the distinct banding patterns of TDP-43 CTFs in the sark-insoluble extracts from the brains of patients with different FTLD-TDP subtypes (lanes type A, B and E) and the GFP-NLSm expressing cells (Dox+) transduced. The corresponding FTLD-TDP extracts also are shown here

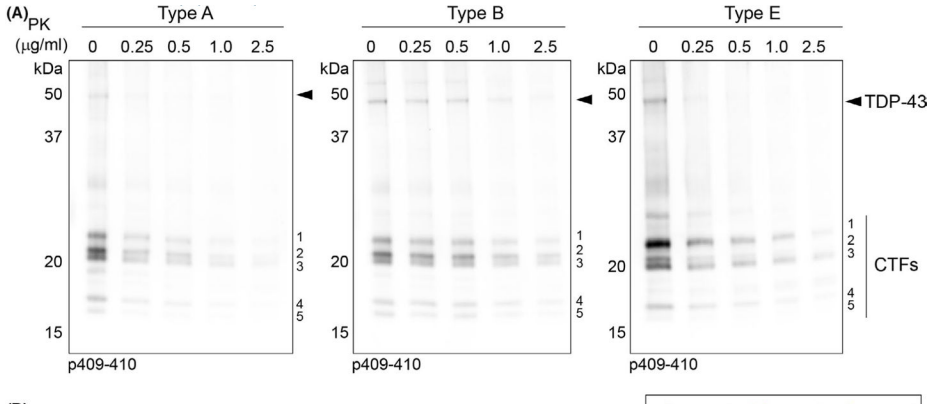

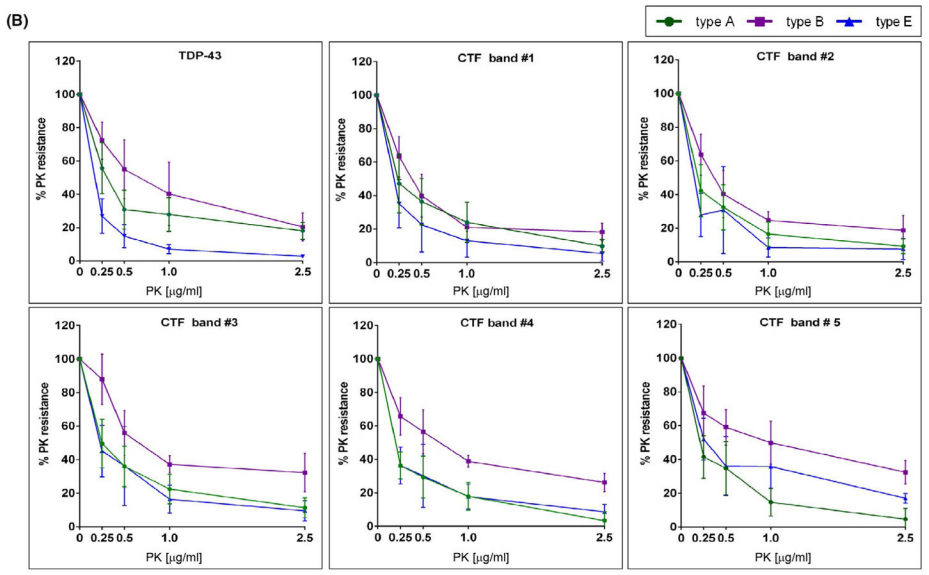

(C)

		Value	Std.Error	DF	t-value	p-value
TDP-43	(Intercept)	2.59	0.57	38	4.55	0.000
	type AB	-1.49	0.68	8	-2.19	0.060
	pk	-1.25	0.31	38	-4.03	0.000
	type AB:pk	0.86	0.37	38	2.33	0.025

		Value	Std.Error	DF	t-value	p-value
CTF band #1	(Intercept)	2.92	0.59	38	4.99	0.000
	type AB	-1.95	0.70	8	-2.79	0.024
	pk	-1.31	0.33	38	-3.98	0.000
	type AB:pk	0.93	0.39	38	2.37	0.023

FIGURE 4.

Differences in PK resistance of insoluble TDP-43 protein between different FTLD-TDP subtypes. (A) Representative immunoblots show the digestion pattern of TDP-43 protein of sark-insoluble brain extracts (type A, type B and type E) treated with proteinase K (PK) using the p409–410 antibody. The different concentrations of PK (μg/ml) used in the assay are labelled in each lane. Molecular weight markers in kDa are shown on the left. Immunoblot show showed the presence of the full-length TDP-43 protein with a Mr of ~43 kDa (arrowhead) and the characteristic CTFs resulting from partial proteolysis including three major bands with a theoretical Mr ranging between ~20–26 kDa (bands #1, #2 and #3) and two minor bands at ~18–19 kDa (bands #4 and #5) on the right. (B) The signal of each p409–410-positive TDP and CTF band was quantified at each PK concentration as a percentage of the initial sample (PK = 0) and plotted as a percent of the PK resistance (%). Plots show the mean values (type A $n = 4$ cases, type B $n = 3$ cases, type E $n = 3$ cases) and

whiskers SEM. (C) A linear mixed-effects model shows statistically significant differences in PK resistance of full-length TDP-43 proteins (TDP-43) and the C-terminal fragment with lower electrophoretic mobility (band #1) in type E extracts relative to type A and B extracts (TDP-43 $p = 0.025$, CTF band #1 $p = 0.023$)

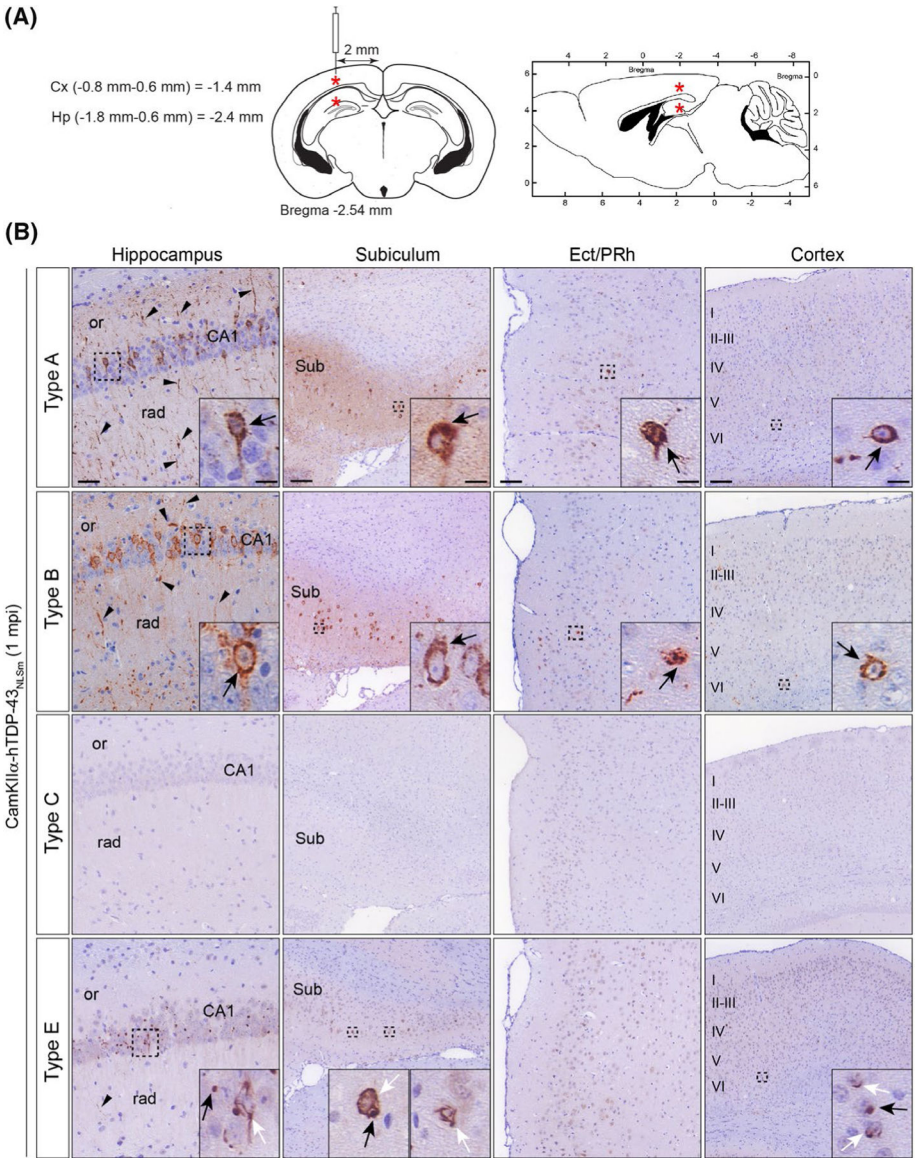

FIGURE 5.

Brain-derived TDP-43 strains from different FTLD-TDP subtypes have distinct seeding properties *in vivo*. (A) Schematic illustrations of coronal and sagittal brain sections (left and right respectively) with coordinates used for the stereotaxic injections into the brains of CamKIIa-hTDP-43$_{NLSm}$ mice. Red asterisks indicate the injection site in the hippocampus and overlying cortex. (B) Representative photomicrographs of p409–410 immunostaining of phospho-TDP-43 in coronal brain sections from CamKIIa-hTDP43$_{NLSm}$ mice stereotaxically injected with human brain-derived TDP-43 protein extracts from different FTLD-TDP subtypes; type A, type B, type C and type E at 1 mpi. Images show p409–410-positive staining in the ipsilateral hippocampus (cornu amonis (CA1 layer), stratum radiatum (rad), and oriens (or)), in the subiculum (Sub), in the ectorhinal/perirhinal cortex (Ect/PRh) and neocortex (cortex, layers I–VI). Black arrowheads point to p409–410-positive neuronal processes in the neuropil. Insets show higher magnifications of the black-

dashed boxes. In type A and B injected mice, black arrows point to neurons with intensely stained cytoplasmic p409–410-positive aggregates. In type E injected mice, black arrows point to p409–410-positive dot-like inclusions and white arrows point to p409–410-positive skein-like aggregates

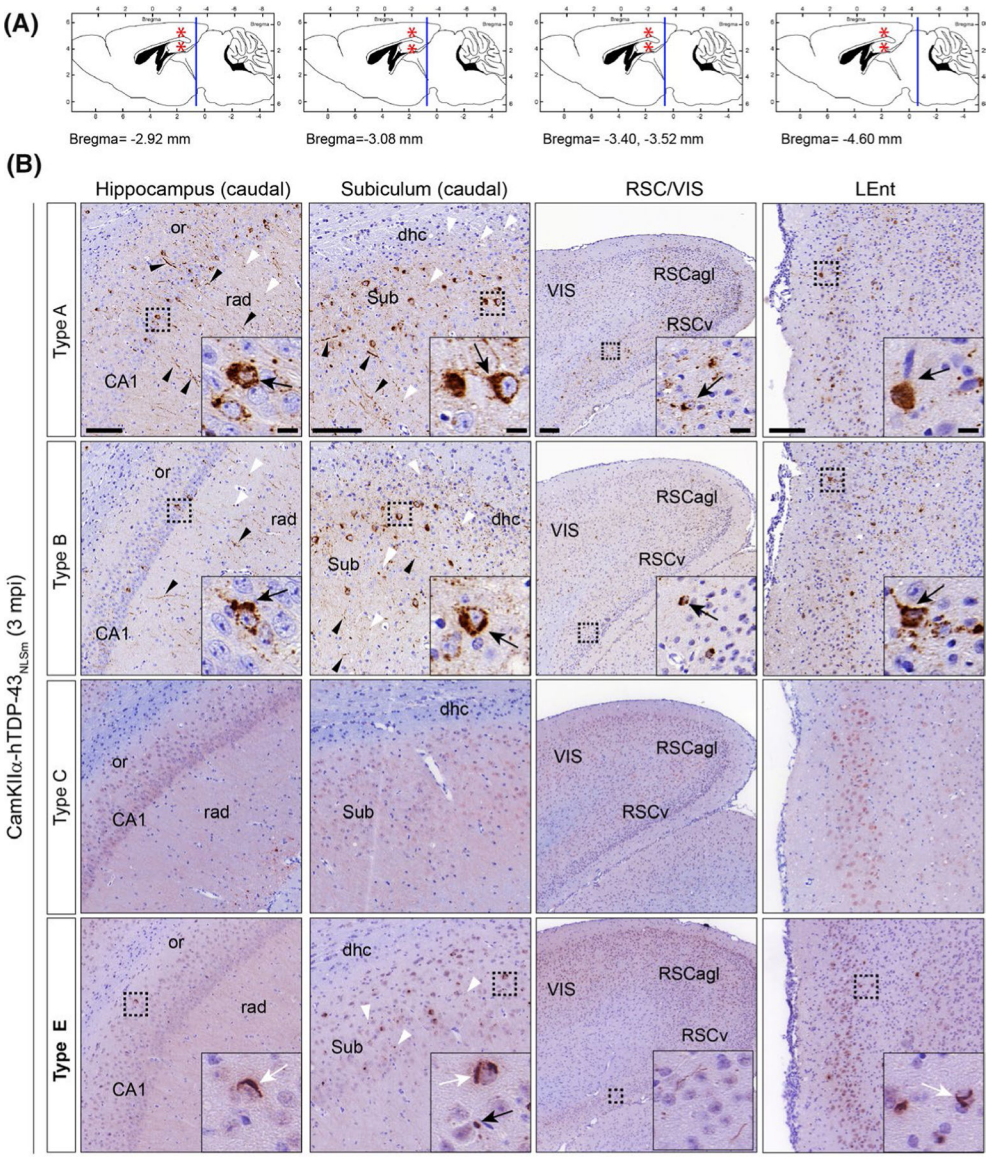

FIGURE 6.

TDP-43 pathology induced in the brain of CamKIIa-hTDP-43$_{NLSm}$ mice injected with brain-derived TDP-43 from different FTLD-TDP subtypes exhibited distinctive spreading patterns over-time. (A) Panels illustrate sagittal brain views of the mouse brain. The red asterisks indicate the injection site in the hippocampus and overlying cortex. Blue lines indicate the localization of the coronal brain sections corresponding to images in B; hippocampus (caudal) (Bregma −2.92 mm), subiculum (caudal) (Bregma −3.08 mm), restrosplenial cortex and primary visual cortex (RSC/VIS) (Bregma −3.40 and −3.52 mm), and lateral entorhinal cortex (LEnt) (Bregma −4.60 mm). (B) Representative photomicrographs of mAb p409–410 immunostaining in coronal brain sections from CamKIIa-hTDP43$_{NLSm}$ mice stereotaxically injected with human brain-derived TDP-43 from different FTLD-TDP subtypes; type A, type B, type C, and type E at 3 mpi. Images show p409–410 positive staining in the ipsilateral side of the brain, in caudal areas distal

from the injection site such as; hippocampus (cornu amonis (CA1 layer), stratum radiatum (rad), and oriens (or)), subiculum (sub) and including the dorsal hippocampal commissure (dhc), ventral and lateral agranular RSC (RSCv and RSCagl), VIS and LEnt. Black arrowheads point to p409–410 positive short and long neurites and white arrowheads to dotted staining in the neuropil. Insets show higher magnifications of the black-dashed boxes; in type A and B injected mice, black arrows point to neurons with widespread cytoplasmic p409–410 positive aggregates whereas in type E injected mice, black arrows point to dot-like inclusions and white arrows skein-like aggregates. Scale bar = 100 μm, and 10 μm (insets)